Measuring the Change in the Intermolecular Raman Spectrum during Dipolar Solvation

David F. Underwood and David A. Blank*

Department of Chemistry, University of Minnesota, 207 Pleasant St. SE, Minneapolis, Minnesota 55455

Received: December 21, 2004; In Final Form: February 23, 2005

We demonstrate a method to directly measure the change in the spectrum of intermolecular solvent fluctuations as a function of time after electronic excitation of a solute, and this method is applied to the dye Coumarin 102 (C102) in acetonitrile. The complete intermolecular response is captured following resonant excitation with time domain third-order Raman spectroscopy. In a previous report, we introduced this method and used it to probe one point in the intermolecular response as a function of time after solute excitation (Underwood, D. F., Blank, D. A. *J. Phys. Chem. A* **2003**, *107* (7), 956). Here we extend this approach to recover the change in the entire intermolecular response as a function of time. To our knowledge the results provide the first direct measurement of the difference in the equilibrated intermolecular response after excitation of a solute and its evolution during a dipolar solvation event. Excitation of C102 results in a significant increase in the solvent−solute interaction due to a large increase in the dipole moment. The observed change in the intermolecular response is consistent with a rapid change in local solvent density, with intermolecular kinetic energy transfer changing the response on longer time scales. Evolution of the response exhibits a strong frequency dependence and suggests changes over longer distances at longer delay times. The measured change in the spectrum of solvent fluctuations represents a direct experimental confirmation of the breakdown of linear response and confirms predictions from molecular dynamics simulations.

1. Introduction

The importance of solvation dynamics in condensed phase chemical reactions has long been appreciated and has received considerable attention (for example, see refs 1−4). More recent time-resolved studies have focused on the ultrafast dynamics associated with reorganization of the solvent in response to impulsive electronic rearrangement in a solute. The solvent response is typically followed spectroscopically via the effect of the local environment on a solute's electronic energy gap. Techniques such as time-dependent fluorescence Stokes shift and three pulse echo peak shift (3PEPS) have revealed the multitude of time scales associated with solvent reorganization, and comparisons with simulations have led to significant insights into the solvent motions responsible for the observed responses.[5−9]

Reliance on the electronic energy gap correlation function, which we will refer to as $S(t)$, as a probe of the solvent response, has the advantage of providing the solute's perspective of the local environment. For example, this offers a direct probe of the dynamics associated with phenomena such as line broadening. However, since it is the gap that is measured as a function of time, it is the combined effect of the solvent fluctuations on both the ground and excited states of the solute that are observed. As a result, assumptions concerning the correlations between both the equilibrium and nonequilibrium fluctuations around both of the solute electronic states are required when considering the relationship between the solvent fluctuations and $S(t)$. The linear response approximation, LR, is often evoked to help address this issue, including the assumptions that solvent fluctuations around the excited electronic state are the same as those around the ground electronic state.[10−15] However, while applications of LR have often demonstrated agreement with experiment, recent simulations have illustrated potentially common failures.[10,11,14−20] The failure of LR is perhaps less surprising than the apparent initial success given the large change in the solvent−solute interaction that often accompanies the change in solute electronic state. This means that the perturbations driving nonequilibrium solvation are not small, as assumed in LR, and that the equilibrium solvent fluctuations around the ground and excited state of the solute respectively are quite different.[11,14,15]

The dynamics associated with the failure of LR, such as the evolution of the local solvent fluctuations, are likely to play an important role not only in basic solvation events, but in reactive dynamics such as charge transfer as well.[1−4] The difficulty in experimentally accessing the assumptions associated with LR via resonant solute probes is due, in part, to the fact that measurements of $S(t)$ provide limited direct information concerning the *changes* in the intermolecular spectrum of motions that accompany electronic rearrangement in a solute. Experiments that probe the solvent directly can provide a complementary perspective, and if the complete intermolecular response can be measured as a function of time after solute excitation, the question of how fluctuations in the local environment are changing can be addressed. Sub-picosecond THz pulses[21−23] and polarizability response spectroscopy[24] have been used to directly probe the one-dimensional solvent response that is driven by excitation of a solute. Schmuttenmaer and co-workers have also recovered the spectrum of the THz probe as a function of delay time after excitation of a chromophore in solution. Spreading the intermolecular response into a second dimension allowed them to resonantly interrogate the transient change in the solvent spectrum between 3 and 100 cm^{-1} following excitation of the cyanine dye TBNC in solution.[25−28] TBNC was specifically selected to look at an electronic transition that resulted in almost no change in the solute's dipole moment to minimize signal

* To whom correspondence should be addressed. E-mail: blank@chem.umn.edu. Phone: (612) 624-0571. Fax: (612) 624-1589.

10.1021/jp044187i CCC: $30.25
Published on Web 03/24/2005

contributions from the solute. The fact that dynamic electronic reorganization in the solute can act as a source of THz emission can offer unique insights when applied to charge-transfer events.[25] However, such responses from the solute can complicate the direct probing of the intermolecular solvent response associated with charge transfer and dipolar solvation.

Our research group recently introduced an experimental approach that uses time domain electronically nonresonant third-order Raman spectroscopy to directly measure the change in the intermolecular solvent response following resonant excitation of a solute.[29−32] We refer to this method as RaPTORS, an acronym for Resonant Pump Third-Order Raman probe Spectroscopy. RaPTORS is analogous to the two-dimensional THz experiment; however, the spectrum of solvent motions at a given delay after resonant excitation are experimentally spread into a second time dimension rather than frequency dimension. Using a nonresonant probe offers a complementary look at the change in the intermolecular response with some potential advantages. These include broader spectral coverage, higher time resolution, application to liquid samples that are opaque in the THz spectral range, and no interference in probing the solvent response from dynamics in the solute that resonantly emit THz radiation. RaPTORS can measure the solvent response for a wide range of dynamic events in solution, including dipolar solvation and charge-transfer reactions.

In the work reported here we apply RaPTORS to measure the change in the complete intermolecular Raman response during a dipolar solvation event, the excitation of Coumarin 102 (C102) in acetonitrile, CH_3CN. Previously, RaPTORS was applied to follow a single point in the solvent response, for example the maximum of the librational contribution, as a function of time after resonant solute excitation.[29] In addition to following solvation dynamics, this approach was demonstrated to offer a new perspective on an ultrafast excited-state proton-transfer reaction.[30] As discussed in the initial work, the presence of a time-dependent local oscillator, that was incorporated to amplify the signal and provide signal detection at the amplitude level, complicated recovery of the complete intermolecular response as a function of time after solute excitation. In this work, a measurement of the time-dependent local oscillator field is incorporated into a forward convolution analysis of the RaPTORS response, and the result is the determination of the *complete* change in the intermolecular Raman response as a function of resonant excitation delay. The time-dependent change is discussed in terms of the change in the intermolecular solvent−solute interaction following excitation of C102. Our results indicate a rapid increase in local density, slower intermolecular kinetic energy transfer, and a clear difference between the intermolecular response around the ground and excited states. At the end, a comparison is made with the assumptions of linear response.

2. Experimental Section

The laser system and experimental setup for the RaPTORS measurements have been described previously.[29] Briefly, the experiment involves the resonant electronic excitation of a solute followed by three electronically nonresonant laser pulses that probe the low frequency (1−500 cm^{-1}) Raman spectrum in the time domain. Figure 1 shows the time ordering and labels used for the pulse sequence and the phase matching geometry employed. The resonant and nonresonant laser fields are labeled E_r and E_{nr1-3} respectively. We refer to the time delay between the resonant excitation pulse and the time coincident first two nonresonant laser pulses as t, and the intrinsic delay in the

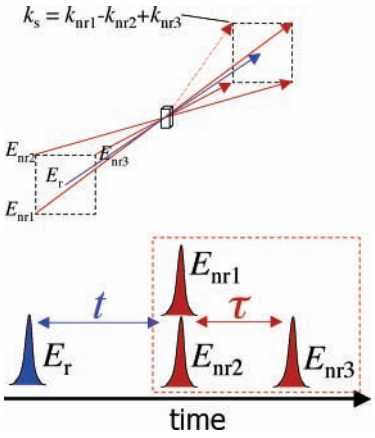

Figure 1. Diagram of the pulse sequence showing the time variable definitions and wavevector matching geometry for the RaPTORS experiments.

nonresonant Raman probe between $E_{nr1,2}$ and E_{nr3} as τ. The nonresonant pulses were arranged in a box geometry, the resonant pulse propagates down the center of the box, and the signal is detected along the phase-matched direction determined by the three nonresonant probe pulses, $k_s = k_{nr1} - k_{nr2} + k_{nr3}$. The resonant laser pulses are chopped with a slotted wheel at 500 Hz, one-half the laser repetition rate, and the resulting modulation of the detected signal field was collected via lock-in detection (SR810, Stanford Research). The RaPTORS response was determined to be linearly dependent on each incoming nonresonant laser field, as well as the concentration of C102, and is considered in detail in Section 3.

The time domain intensity profile of the nonresonant laser pulses, centered at 800 nm, were Gaussian in shape with a full width at half-maximum, fwhm, of 36 fs as determined by three-pulse transient grating measurements in a 1 mm fused silica window placed at the sample location. The resonant pulse was generated by type-I frequency doubling a portion of the 800 nm light in a 1 mm β-BaB_2O_4 (BBO) crystal (CXK Optronics) and compressed using a pair of fused silica prisms. The resulting 400 nm pulses were measured by difference frequency mixing with one of the 800 nm pulses in a 0.1 mm BBO crystal placed at the sample position. The 400 nm pulse intensity profile was determined by difference frequency generation with the 800 nm fundamental in the same BBO crystal and had a fwhm of 40 fs.

The linear polarizations of the nonresonant laser fields were set to suppress the instantaneous electronic response that occurs for $\tau = 0$.[33] The first two nonresonant pulses, E_{nr1} and E_{nr2}, were parallel, E_{nr3} was rotated +45°, and the signal field was polarization selected at −71° relative to E_{nr1} and E_{nr2}. The resulting measured third-order response is equivalent to measuring a linear combination of the parallel and perpendicular tensorial contributions to the response function, $R^{(3)}_{(-71°)(+45°)xx}(\tau) = R^{(3)}_{xxxx}(\tau) - 3R^{(3)}_{yyxx}(\tau)$.[34] The subscripts indicate the polarizations of the individual laser fields and signal listed in reverse order by convention, x and y indicate orthogonal polarizations, and the angles are measured relative to x. The signal was passed through an 800 ± 25 nm band-pass filter and detected using a fast silicon photodiode (Thor-Labs DET210).

In addition to the RaPTORS measurements, electronically nonresonant third-order responses of our samples were measured under identical conditions with the resonant laser field blocked. The signals were heterodyne detected by recombining E_{nr3} with the detected signal field after the sample, as outlined by Tokmakoff and co-workers.[35−37] The phase of the local oscillator

was adjustable by rotation of a microscope cover slip placed prior to recombination with the signal field. Responses were collected with the local oscillator in phase with the signal field and rotated by 180°. The measured signal intensity was reported as the difference between in phase and 180° out of phase to eliminate any residual homodyne contributions.[35] The heterodyne detected nonresonant third-order response is discussed in more detail in Section 3.1.

Room-temperature samples of Coumarin 102 in CH_3CN were flowed at about 0.5 mL/s through a 1 mm thick sample cell with fused silica windows (Starna Cells, # 48-Q-1). The samples had an optical density of 0.4 at 400 nm, indicating a concentration of ~0.5 mM. Coumarin 102 was used as received from Exciton, and spectroscopic grade CH_3CN was used as received from Aldrich Chemical.

Optimized gas-phase structures for C102 were calculated in Gaussian 98 at the B3LYP/Midi! level,[38] which were used to determine CM2 dipole moments in acetonitrile for ground and excited states (SM5.42R/INDO/S2, VEM42/INDO/S2 calculations respectively) using the ZINDO-MN program.[39]

3. Data Analysis and Results

The pulse sequence and definition of time variables t and τ are shown in Figure 1. In the RaPTORS experimental configuration, the signal is measured along the phase-matched direction determined by the three nonresonant probe fields, $k_s = k_{nr1} - k_{nr2} + k_{nr3}$. The resonant pump field, E_r, is modulated and the intensity difference between the signal with and without E_r is monitored.[29]

$$I_{\mathrm{RaPTORS}}(t,\tau) = I_{\text{pump present}}(t,\tau) - I_{\text{no pump}}(\tau) \qquad (1)$$

When the pump pulse is blocked the signal is the nonresonant third-order Raman (TOR) response, which is dominated by the bulk solvent. The signal intensity is the square of the radiated third-order signal field, $E^{(3)}_{\mathrm{solvent}}(\tau)$.

$$I_{\text{no pump}}(\tau) = \left(\frac{nc}{4\pi}\right)\left| E^{(3)}_{\mathrm{solvent}}(\tau)\right|^2 \qquad (2)$$

When the pump pulse is present, the signal intensity is the square of the sum of the third-order signal field from the bulk solvent and some change in that third-order signal field due to the resonant pump pulse, $\Delta E^{(3)}(t,\tau)$.

$$I_{\text{pump present}}(t,\tau) = \left(\frac{nc}{4\pi}\right)\left| E^{(3)}_{\mathrm{solvent}}(\tau) + \Delta E^{(3)}(t,\tau)\right|^2 \qquad (3)$$

Combining eqs 1, 2, and 3,

$$I_{\mathrm{RaPTORS}}(t,\tau) = \left(\frac{nc}{4\pi}\right)\{Re[E^{(3)*}_{\mathrm{solvent}}(\tau)\Delta E^{(3)}(t,\tau)] + |\Delta E^{(3)}(t,\tau)|^2\} = I^{\mathrm{hetero}}_{\mathrm{RaPTORS}}(t,\tau) + I^{\mathrm{homo}}_{\mathrm{RaPTORS}}(t,\tau) \qquad (4)$$

where we have labeled the cross term as the heterodyne detected intensity and the modulus squared change as the homodyne detected intensity. Assuming that the change is small, $\Delta E^{(3)}(t,\tau) \ll E^{(3)}_{\mathrm{solvent}}(\tau)$, the resulting measured signal intensity will be dominated by the heterodyne contribution,

$$I_{\mathrm{RaPTORS}}(t,\tau) \approx I^{\mathrm{hetero}}_{\mathrm{RaPTORS}}(t,\tau) = \left(\frac{nc}{4\pi}\right)Re[E^{(3)*}_{\mathrm{solvent}}(\tau)\Delta E^{(3)}(t,\tau)] \qquad (5)$$

The nonresonant third-order field from the bulk solvent acts as a time-dependent local oscillator in the detection of the desired two-dimensional change induced by the pump pulse, $\Delta E^{(3)}(t,\tau)$. In addition to providing amplification of the desired two-dimensional signal, the local oscillator also provides phase selection. The electronically nonresonant solvent signal, $E^{(3)}_{\mathrm{solvent}}(\tau)$, is real, and as a result this local oscillator amplifies only the electronically nonresonant portion of the change in the third-order Raman response.

The two-dimensional change in the third-order field, $\Delta E^{(3)}(t,\tau)$, is formally the result of interference, i.e., heterodyning with a fifth-order signal field that is scattered along the same direction as $E^{(3)}_{\mathrm{solvent}}(\tau)$, and involves two additional interactions with the resonant pump pulse, $k_{s'} = k_r - k_r + k_{nr1} - k_{nr2} + k_{nr3}$. This is analogous to resonant pump−probe experiments where a third-order signal field is scattered along the same direction as the detected probe laser and the resulting interference is often described as a heterodyne detected linear change in the probe field due to increased absorption or stimulated emission following the action of the pump field.[40] Here we adopt a similar approach and interpret our measurements as the heterodyne detected change in the third-order signal field induced by the action of the resonant pump field.

The third-order signal field, $E^{(3)}(\tau)$, can be related to the nuclear dynamics of the solution via a third-order material response function, $R^{(3)}(\tau)$.[40] In the impulsive limit the third-order response can be expressed as a polarizability correlation function,

$$R^{(3)}(\tau) = -\frac{i}{\hbar}\langle[\alpha(\tau),\alpha(0)]\rangle \qquad (6)$$

The change in the signal field in response to absorption of the resonant pump pulse can then be directly related to the change in the electronically nonresonant response function, eq 6,

$$\Delta E^{(3)}(t,\tau) \propto \Delta R^{(3)}(t,\tau) \qquad (7)$$

and it is this change in the bare nuclear response function that is extracted via analysis of the raw RaPTORS data as described below.

The data analysis is considered in three parts. The intent is to extract the change in the nonresonant third-order response as a function of both t and τ from the measured RaPTORS response, eq 4. In section 3.1, the nonresonant third-order response of the solvent, $R^{(3)}_{\mathrm{solvent}}(\tau)$, the local oscillator in the RaPTORS measurements, is determined by fitting a heterodyne-detected nonresonant TOR measurement. Next, the RaPTORS measurements are addressed. The time dependence of the local oscillator along the τ time variable leads to greater complexity when considering the dynamics in this dimension relative to the response along t, where the local oscillator is time *in*dependent. As a result the analysis of the dynamics along each of the two time dimensions is considered separately, sections 3.2 and 3.3. In section 3.3, $R^{(3)}_{\mathrm{solvent}}(\tau)$ determined in section 3.1 is used to generate the time-dependent local oscillator in a forward convolution fitting approach to the determination of $\Delta R^{(3)}(t,\tau)$ along τ for a series of delays after the resonant pump pulse, t.

3.1. The Electronically Nonresonant Third-Order Response, $R_{\mathrm{solvent}}^{(3)}(\tau)$. The nonresonant third-order response for the sample is measured in a heterodyne detection geometry as described in section 2. The data are presented as the difference of two scans where the local oscillator has been phase shifted by 180°. This subtraction eliminates any residual homodyne components in the signal and leaves only the cross term between

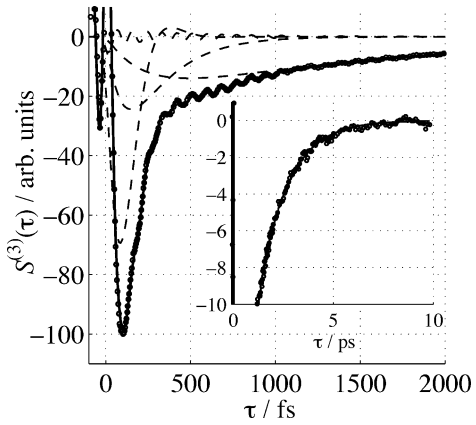

Figure 2. The heterodyne-detected third-order Raman response for CH_3CN. The circles are the raw data points, and the solid line is the complete fit using the bare response function in Figure 3 and eq 9. The dashed lines are the four individual Brownian oscillator components of the fit, shown in Figure 3 and described in Table 1.

the third-order signal field and the local oscillator field.[35] The heterodyne detected electronically nonresonant third-order signal is then related to the third-order response function via integration over the temporal envelopes of the laser pulses,[40]

$$I_{\text{solvent}}(\tau) \propto \int_0^\infty \mathrm{d}t' E^*_{\text{LO}}(t') E_{\text{nr3}}(t') \times \int_0^\infty \mathrm{d}t'' R^{(3)}(t'') E^*_{\text{nr2}}(t' - t'' + \tau) E_{\text{nr1}}(t' - t'' + \tau) \quad (8)$$

In this case the local oscillator field is provided by the third nonresonant laser pulse, $E_{\text{LO}}(t') = E_{\text{nr3}}(t')$. Since all three nonresonant field envelopes are identical, the expression can be written as a convolution over the pulse intensity autocorrelation function[41−45]

$$I_{\text{solvent}}(\tau) \propto \int_{-\infty}^\infty \mathrm{d}t'' R^{(3)}(t'') \int_{-\infty}^\infty \mathrm{d}t' I_{\text{nr}}(t') I_{\text{nr}}(t' - t'' + \tau) \quad (9)$$

The pulse intensity envelopes were determined as described in section 2. To model the third-order response function, the electronic polarizability of the system is expanded in a set of nuclear coordinates, q_i,

$$\alpha(\tau) = \alpha(q_0) + \sum_i \alpha_i^{(1)} q_i + \ldots \quad (10)$$

where $\alpha_i^{(1)} = (\partial\alpha/\partial q)_{q_0}$. Inserting eq 10 into eq 6, and assuming that the first-order term is the dominant term, the third-order response function can be expressed as a sum of vibrational correlation functions, $G_i(\tau) = \langle q_i(\tau) q_i(0) \rangle$,

$$R^{(3)}(\tau) = \sum_i |\alpha_i^{(1)}|^2 G_i(\tau) \quad (11)$$

The individual vibrational correlation functions are modeled with Brownian oscillators, which provide a qualitative description of overdamped intermolecular motions and vary continuously from overdamped to underdamped vibrations.[40]

$$G_i(\tau) = \eta_i \sin(\Omega_i \tau) \exp(-\Lambda_i \tau) \quad (12)$$

The reduced frequency is defined as $\Omega_i = \sqrt{\omega_i^2 - \Lambda_i^2}$, with damping $\Lambda_i = \gamma_i/2$. Since the adjustable relative amplitude of each oscillator is provided by the Raman weight in eq 11, $|\alpha_i^{(1)}|^2$, η_i in eq 12 was restricted to ± 1 to indicate the sign of the response. For the laser polarization conditions in this experiment, $R^{(3)}_{(-71°)(+45°)xx}(\tau) = R^{(3)}_{xxxx}(\tau) - 3R^{(3)}_{yyxx}(\tau)$, the overdamped intermolecular response should be negative,[34] and this is consistent with the sign of our measured signal.

TABLE 1: Brownian Oscillator Fitting Parameters Used To Construct the Third-Order Response Function, $R^{(3)}_{\text{solvent}}(\tau)$[a]

oscillator	η	$\alpha^{(1)}$	ω/cm^{-1}	γ/cm^{-1}
1	−1	0.30	9.48	28.0
2	−1	0.71	36.5	81.2
3	−1	1.57	78.9	111.4
4	−1	1.15	379	18.4

[a] See eqs 11 and 12, and Figure 3.

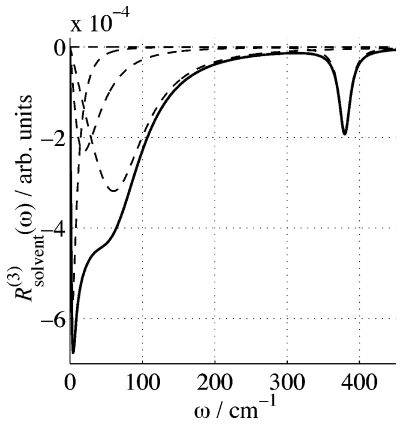

Figure 3. The sin transform of the bare third-order response function, $\mathrm{Im}[\mathcal{F}\{R^{(3)}_{\text{solvent}}(\tau)\}]$, determined by a forward convolution fit of the data for CH_3CN in Figure 2 using eq 9. The solid line is the total response, and the dashed lines are the individual Brownian oscillator components described in Table 1.

The third-order response function for CH_3CN was modeled as a collection of four Brownian oscillators and an instantaneous response at $\tau = 0$, which was included to model the residual electronic response. The data were simulated using eq 9, and iterative adjustment of the Brownian parameters used to construct $R^{(3)}_{\text{solvent}}(\tau)$ was performed to determine an optimized fit. The fit is shown along with the heterodyne detected third-order signal in Figure 2. The fitting parameters are listed in Table 1 and the sin transform of the bare time domain response function, $R^{(3)}_{\text{solvent}}(\omega) = \mathrm{Im}[\mathcal{F}\{R^{(3)}_{\text{solvent}}(\tau)\}]$, is plotted in Figure 3. The overdamped portion of the spectrum agrees well with previous heterodyne detected optical Kerr measurements.[46−51] The underdamped beat at 379 cm^{-1} is the intramolecular bending mode in acetonitrile. We note that within the signal-to-noise of our experiment there was not a detectable difference in $R^{(3)}_{\text{solvent}}(\tau)$ for neat samples of CH_3CN and the samples containing the C102 chromophores used in the RaPTORS measurements described in the following sections. As a result, we assume that the nonresonant solvent response is identical with and without the inclusion of C102 under the conditions used in this work.

3.2. RaPTORS Measurements along *t* for Fixed Values of *τ*. The solvent response in eq 5, $E^{(3)}_{\text{solvent}}(\tau)$, provides a time *in*dependent local oscillator when considering RaPTORS measurements as a function t for fixed values of τ. As a result, the t dependence for a fixed value of τ can be simulated directly as a convolution of $\Delta R^{(3)}(t;\tau)$ with the instrument response in the t dimension, $N(t)$,

$$I_{\text{RaPTORS}}(t;\tau) \propto \int_{-\infty}^\infty \Delta R^{(3)}(t - t';\tau) N(t') \mathrm{d}t' \quad (13)$$

To allow for both rising and decaying time scales, positive and negative responses, and the significant offset at long time

TABLE 2: Optimized Fitting Parameters Used in Eq 14 To Simulate the RaPTORS Response along *t* for Fixed Values of τ

τ/fs	t_1/fs	B	t_2/ps	C	t_3/ps	D
100	<100	−10.0	14.3	−8.20	65.3	−6.42
150	<100	−44.5	1.2	−38.7	48.0	−29.2
200	<100	−38.7	6.4	−32.7	52.9	−25.3
300	<100	−9.89	12.6	−7.43	68.8	−6.30
500	115	−1.91	22.7	−1.26	103	−1.07

due to the lifetime of the C102 excited-state far exceeding our measurement time, the response along t was modeled as a set of sequential steps,

$$a(t)\ \mathrm{A} \xrightarrow{t_1} b(t)\ \mathrm{B} \xrightarrow{t_2} c(t)\ \mathrm{C} \xrightarrow{t_3} d(t)\ \mathrm{D} \qquad (14)$$

Each step represents evolution between different values of our time dependent response given by A−D. Associated with each value there is a time dependent weight, $a(t)-d(t)$, that varies from 0 to 1. The sum of the weights is restricted to 1 at all t, and initial conditions are defined by the following values: $A = 0$, $a(t = 0) = 1$, $b(t = 0) = 0$, $c(t = 0) = 0$, and $d(t = 0) = 0$. The resulting time dependent signal, $\Delta R^{(3)}(t;\tau)$, is then the weighted sum of the values at each step,

$$\Delta R^{(3)}(t;\tau) = a(t)\ \mathrm{A} + b(t)\ \mathrm{B} + c(t)\ \mathrm{C} + d(t)\ \mathrm{D} \qquad (15)$$

The coupled differential equations that describe the time evolution of $a(t)-d(t)$ and the analytical solution are presented in detail in the Supporting Information. The data were simulated using eq 13 and adjusting the values, B−D, and time constants, $t_1 - t_3$, in eqs 14 and 15 until a reasonable fit was achieved. The optimized fitting parameters are listed in Table 2. Raw data and optimized fits are shown for slices along t at $\tau = 150$ fs and $\tau = 500$ fs in Figure 4. Raw data and fits at the other values of τ are available in the Supporting Information.

The responses from a neat CH_3CN sample under identical conditions are shown as the dashed lines in Figure 4. The neat solvent signal was dominated by an instantaneous response at $t = 0$ and was included as a component in the forward convolution fitting procedure after linear scaling to account for the reduction in optical density at 400 nm that accompanies removal of the C102 chromophore. The instrument response along t is determined by the group velocity miss-match, GVM, between the 400 nm resonant pulses and the 800 nm nonresonant pulses. Fits to the neat solvent response were consistent with the calculated GVM resulting in a Gaussian instrument response function with a fwhm = 140 fs that was used for $N(t)$.

3.3. RaPTORS Measurements along τ for Fixed Values of *t*. Simulation of the RaPTORS response along τ requires inclusion of the third-order solvent signal field, $E^{(3)}_{\mathrm{solvent}}(\tau)$, as a time-dependent local oscillator, see eq 4. The experimental parameters are adjusted such that the signal at a specific point in the two-dimensional response($t = 500$ fs,$\tau = 150$ fs), with the resonant pulse present, eq 3, represents ca. 1% increase over the same conditions with the pump pulse blocked, eq 2. If we assume there are no interfering cross terms when taking the modulus squared in eq 2, then the intrinsic local oscillator, $E^{(3)}_{\mathrm{solvent}}(\tau)$, is ca. 100 times larger than the desired signal, $\Delta R^{(3)}(\tau;t)$, at ($t = 500$ fs, $\tau = 150$ fs). Under these conditions, the approximation in eq 5 is reasonable, and the RaPTORS signal can be considered as the heterodyne term alone. However, since the local oscillator is time-dependent, and at larger values of τ tends toward zero as shown in the insert of Figure 2, the homodyne term is included in the simulations. It will be shown to provide a very small, but measurable contribution for $\tau > 4$ ps.

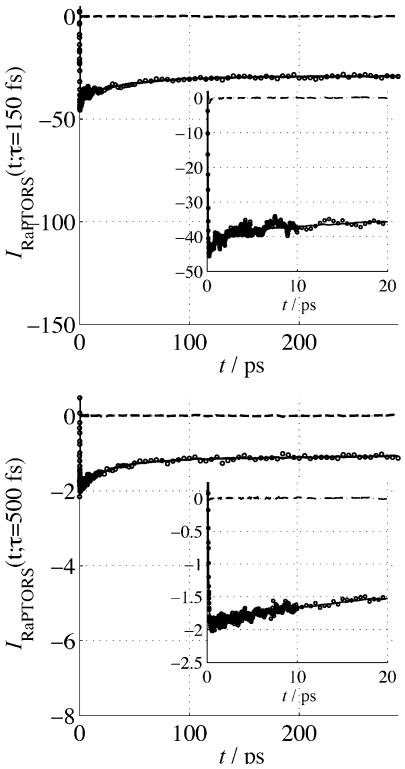

Figure 4. RaPTORS measurements on C102 in CH_3CN along t for $\tau = 150$ fs (top) and $\tau = 500$ fs (bottom). The circles are the raw data, and the solid line is the fit using eqs 13, 14, and 15. The fitting parameters are listed in Table 2. The dashed lines are identical measurements on neat CH_3CN.

The heterodyne contribution, eq 5, is treated in an analogous fashion to the heterodyne detected signal described in eq 8, where the local oscillator in this case is the time-dependent third-order, nonresonant bulk solvent signal field, $E^{(3)}_{\mathrm{solvent}}(\tau)$,

$$I^{\mathrm{hetero}}_{\mathrm{RaPTORS}}(\tau;t) \propto \int_0^\infty \mathrm{d}t' E^*_{\mathrm{solvent}}(t') E_{\mathrm{nr3}}(t') \times \int_0^\infty \mathrm{d}t'' \Delta R^{(3)}(t'';t) E^*_{\mathrm{nr2}}(t' - t'' + \tau) E_{\mathrm{nr1}}(t' - t'' + \tau) \qquad (16)$$

The local oscillator field is then included using the third-order response function for the solvent, $R^{(3)}_{\mathrm{solvent}}$, determined in section 3.1 and shown in Figure 3,

$$E_{\mathrm{solvent}}(t') = iE_{\mathrm{nr3}}(t') \times \int_{-\infty}^\infty \mathrm{d}t'' R^{(3)}_{\mathrm{solvent}}(t'') E^*_{\mathrm{nr2}}(t' - t'' + \tau) E_{\mathrm{nr1}}(t' - t'' + \tau) \qquad (17)$$

Combining eqs 16 and 17, and using the fact that the field envelopes for nonresonant pulses 1 and 2 are identical ($E^*_{\mathrm{nr2}} E_{\mathrm{nr1}} \propto I_{\mathrm{nr}}$),

$$I^{\mathrm{hetero}}_{\mathrm{RaPTORS}}(\tau;t) \propto \int_0^\infty I_{\mathrm{nr3}}(t') \left(\int_0^\infty R^{(3)}_{\mathrm{solvent}}(t'') I_{\mathrm{nr}}(t' - t'' + \tau)\mathrm{d}t''\right) \times \left(\int_0^\infty \Delta R^{(3)}(t'';t) I_{\mathrm{nr}}(t' - t'' + \tau)\mathrm{d}t''\right)\mathrm{d}t' \qquad (18)$$

Following convolution over the laser pulses, the homodyne contribution, the second term on the right-hand side of eq 4, can be expressed as,

$$I^{\mathrm{homo}}_{\mathrm{RaPTORS}}(\tau;t) \propto \int_0^\infty \mathrm{d}t' I_{\mathrm{nr3}}(t') \left|\int_0^\infty \mathrm{d}t'' \Delta R^{(3)}(t'';t) I_{\mathrm{nr}}(t')\right|^2 \qquad (19)$$

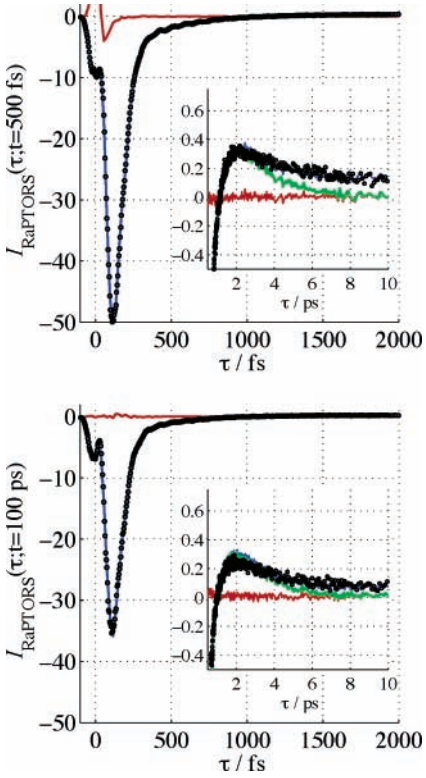

Figure 5. RaPTORS measurements on C102 in CH_3CN along τ for $t = 500$ fs (top) and $t = 100$ ps (bottom). The circles are the raw data, and the blue lines are the fits using $\Delta R^{(3)}$ in Figure 6 and eqs 4, 18, and 19. The red lines are identical measurements on neat CH_3CN. The green lines show the fit without the homodyne contribution using eqs 5 and 18. The residual of the fit at $t = 500$ fs is shown in Figure 7.

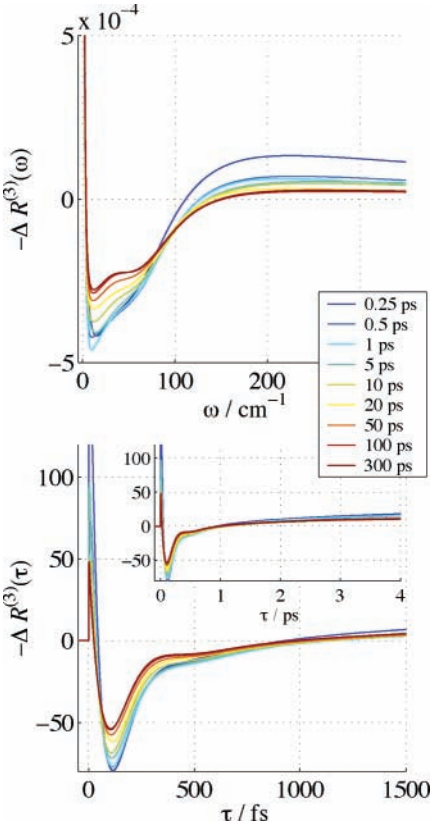

Figure 6. The change in the third-order intermolecular Raman response function following excitation of C102 in CH_3CN. These were determined by forward convolution fitting of the RaPTORS measurements along τ for a series of fixed t values using eqs 4, 18, and 19. Two of the fits are shown in Figure 5, and the rest are available in the Supporting Information section. The top figure is the sin transformation of the change in the third-order response shown in the bottom figure. The legend indicates the fixed value of t.

The total RaPTORS response as a function of τ for a fixed value of t is the sum of the heterodyne and homodyne contributions, eqs 18 and 19, where all of the parameters are determined except the change in the third-order Raman response function, $\Delta R^{(3)}(\tau;t)$.

The change in the third-order response function along τ for a series of time delays t was modeled as a change in the third-order response induced by resonant excitation of C102,

$$\Delta R^{(3)}(\tau;t) = C[R^{(3)}_{\text{pumppresent}}(\tau;t) - R^{(3)}_{\text{nopump}}(\tau)] \qquad (20)$$

$R^{(3)}_{\text{nopump}}(\tau)$ was held fixed and represented by the bulk solvent overdamped nuclear response determined in section 3.1, the sum of Brownian oscillators 1−3 in Table 1. $R^{(3)}_{\text{pumppresent}}(\tau;t)$ was modeled as an instantaneous electronic response and the sum of three overdamped Brownian oscillators. The data were simulated as the sum of eqs 18 and 19, and $R^{(3)}_{\text{pumppresent}}(\tau;t)$ and the scale factor C were varied to optimize the fit to the measure data. The scale factor was restricted to be the same for all values of t. The data and fits for t values of 500 fs and 100 ps are shown in Figure 5, and the $\Delta R^{(3)}(\tau;t)$ determined for all nine values of t measured are shown in Figure 6. Raw data and fits not shown in Figure 5 are available in the Supporting Information. The fits also include a fixed contribution from identical measurements on neat CH_3CN scaled to account for the difference in optical density at 400 nm. This solvent background only contributes to the RaPTORS intensity at small values of both t and τ, and is shown as the red lines in Figure 5.

Optimized fitting parameters used to construct $R^{(3)}_{\text{pumppresent}}(\tau;t)$ are tabulated in the Supporting Information. We emphasize that eq 20 was treated simply as an adjustable function capable of generating a set of $\Delta R^{(3)}(\tau;t)$ that provided high quality fits to the raw data. No restrictions were placed on the individual adjustable Brownian oscillator components in $R^{(3)}_{\text{pumppresent}}(\tau;t)$. The main goal, and the key result of this work, is the determination of the *total* change in the intermolecular response shown in Figure 6. Since the scale factor is restricted to be the same for all values of t, the fits do reflect the relative amplitude of the change at each time point after resonant excitation. One of the advantages of the intrinsic local oscillator is that the absolute amplitude of the change can be estimated from the ratio of the local oscillator and RaPTORS signal intensities. As indicated above this is ca. 1% at delay values of $t = 500$ fs and $\tau = 150$ fs.

In Figure 6, the determined $\Delta R^{(3)}(\tau;t)$ is plotted with an inverted sign. This convention was chosen to indicate increases and decreases in the third-order Raman response as up and down respectively on the vertical axis of the plot. As described in Section 3.1, the polarization of the electronically nonresonant laser fields are set to select a tensorial component of the third-order response that is negative in the case of the intermolecular motions. As a result, increases in the intermolecular response are reflected as decreases (more negative) in the signal. The raw RaPTORS data, such as that shown in Figures 4 and 5, reflects the cross term between $\Delta R^{(3)}(\tau;t)$ and $R^{(3)}_{\text{solvent}}$, eq 5. For either sense of the response dictated by the relative polarizations of the three nonresonant fields, positive or negative, this product remains negative for a decrease and positive for an increase in the intermolecular Raman response.

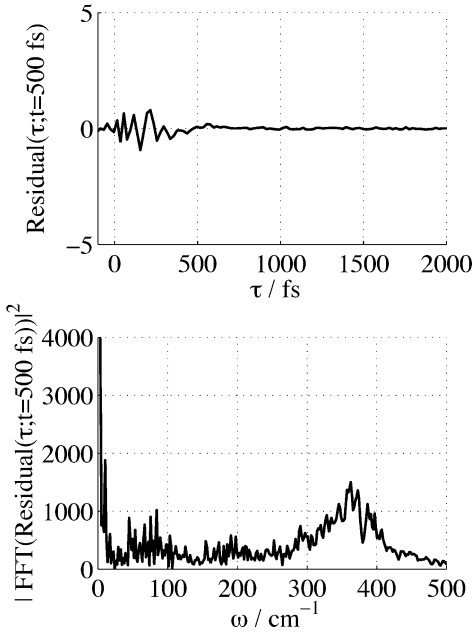

Figure 7. The residual (data − fit) for the RaPTORS scan along τ at $t = 500$ fs shown in the top of Figure 5 (top). The Fourier transform intensity of the residual (bottom).

The green lines in Figure 5 present the fits using only the heterodyne component of the response, eq 5. There is no significant difference between this fit and the blue lines where the homodyne term has been included, eq 5, for $\tau < 4$ ps. This indicates that the assumption $\Delta E^{(3)}(\tau;t) \ll E^{(3)}_{\text{solvent}}(\tau)$ is reasonable for this part of the response. However, for $\tau > 4$ ps it is clear that the small remaining signal is dominated by the homodyne contribution, and this is a direct result of the very small amplitude of the time-dependent local oscillator, $E^{(3)}_{\text{solvent}}(\tau)$, beyond 4 ps, see Figure 2. The determined $\Delta R^{(3)}(\tau;t)$ reported in Figure 6 are restricted to the region where the homodyne contribution to the response is minimal.

No underdamped motions were included in the optimized $\Delta R^{(3)}(\tau;t)$. The bending motion at 379 cm^{-1} shown in Figure 3 was included in the local oscillator and accounts for the majority of the underdamped beats exhibited in the data along τ. However, the residual of the fit at $t = 500$ fs is shown in Figure 7 and does indicate that a small underdamped motion remains in $\Delta R^{(3)}(\tau;t)$. This motion is centered near the CH_3CN bending frequency at 380 cm^{-1} and damps very rapidly. Although this result is consistent with a slight shift of the bend to higher frequency following C102 excitation, the presence of the CH_3CN bending in the time-dependent local oscillator makes a quantitative interpretation of the residual motion difficult. With no evidence for a change in any underdamped motions at frequencies other than the solvent bending vibration, we limit the discussion of our results to the change in the intermolecular response.

4. Computational Results

To consider the change in the intermolecular response in the context of the change in the C102−CH_3CN intermolecular interaction, the bimolecular interaction energy between the neutral solute and solvent were calculated. The bimolecular solvent solute interaction energy as a function of separation distance $U(r)$ is expressed as the sum of the electrostatic (dipole−dipole), induction (dipole − induced dipole) and dispersion interactions respectively,[24,52,53]

$$U(r) = -\frac{1}{r^6}\left\{\frac{2\mu_1^2\mu_2^2}{3kT(4\pi\epsilon_0)^2} + \frac{\mu_1^2\alpha_2 + \alpha_1\mu_2^2}{(4\pi\epsilon_0)^2} + \frac{3\alpha_1\alpha_2}{2(4\pi\epsilon_0)^2}\frac{E_1^{\text{I}}E_2^{\text{I}}}{(E_1^{\text{I}} + E_2^{\text{I}})}\right\}. \quad (21)$$

As evident from eq 21, six variables are required for this calculation, they are the dipole moments, μ_{S_0,S_1}, electronic polarizabilities, α_{S_0,S_1}, and ionization potentials, $E^{\text{I}}_{S_0,S_1}$, where the subscripts indicate the ground and/or excited state. To calculate these numbers, we used the ZINDO-MN method, with solvent parameters taken from the Minnesota Solvent Descriptor Database. This method allows direct determination of dipole moments and orientationally averaged polarizability values (ground and excited states) for C102 in a model acetonitrile environment. We note that many computational results have been published previously for C102 and similar coumarins;[54−58] however, since we are concerned specifically with the interaction energy between C102 and surrounding acetonitrile molecules, we chose to employ a computational method that includes the electrostatic effect of the solvent in the determination of μ_{S_0,S_1} and α_{S_0,S_1} for C102. The change in ionization potential was determined via gas-phase B3LYP/Midi! results for the ground state, minus the energy added to the chromophore through absorption of a 400 nm photon. We note that our results qualitatively agree with recent high-level calculations by Castner and co-workers,[54] where these parameters were calculated for C102 in solvents other than acetonitrile. In both states, the interaction is dominated by the electrostatic dipole−dipole interaction and the change is likewise dominated by the change in the electrostatic term.

5. Discussion

Although the overdamped intermolecular response in solution is continuous and largely featureless, the bimodal character of the response is well established (for examples see refs 6, 7, 9, 18, 58, 59). Figures 2 and 3 show the bimodal character exhibited by the intermolecular spectrum of bulk CH_3CN. The faster component in the response is often associated with single molecule reorientational motion, librations, and the slowest component is assigned to diffusive solvent reorganization. The role of collision-induced contributions to the TOR response, which can result from both orientational motions and density fluctuations, has received considerable attention.[18,60−67] The time scales of density fluctuations can be comparable to librations,[68−71] and the relative contributions of the librational, collision-induced and cross-terms between these components in the TOR response remains a topic of study.

When considering whether there were two or three resolvable intermolecular contributions, we found the use of three overdamped components to represent the TOR response in Figure 2 improved the fit when compared to the optimization of only two overdamped Brownian oscillators. Defining the three response types by using different simple dynamical models for each, Scherer and co-workers assigned a set of three responses in the optical Kerr effect spectrum of CH_3CN to librations, collision-induced, and diffusive reorganization.[24] The three resulting components are very similar to the three overdamped Brownian oscillators in Figure 3, and we adopt the same assignment of these contributions to the TOR response. However, since the librational and translational, and the translational and diffusive responses are predicted to significantly overlap in time, separation of these components in the TOR spectrum is under-determined and significantly influenced by the model(s)

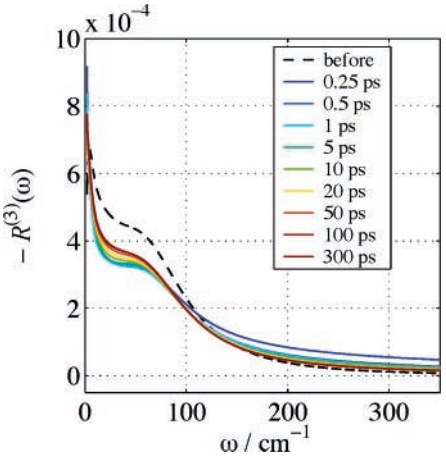

Figure 8. The third-order intermolecular Raman response function before and after excitation of C102. The "before" response is assumed to be the response of the bulk solvent from Figure 3 and the "after" response is created from $\Delta R^{(3)}(\omega;t)$ in Figure 6 as described in Section 5. The legend indicates the fixed value of time delay t.

employed. The discussion here will focus on the total measured intermolecular spectrum and the change in that spectrum induced by excitation of C102. The overlapping contributions are considered only qualitatively as librations in the highest frequency component peaked around 60 cm^{-1}, collision-induced contributions in the middle, peaked around 18 cm^{-1}, and diffusive reorganization at the low frequencies, peaked around 4 cm^{-1}.

Figure 6 presents the difference in the intermolecular Raman response between the excited and ground electronic states of C102 in CH_3CN for a series of delay times after excitation of C102. Generally, the change in the electronic state of C102 results in a decreased response for motions in the middle of the intermolecular spectrum, 3−110 cm^{-1}, and an increase for the motions at the outsides of the intermolecular spectrum, less than 3 cm^{-1} and greater than 110 cm^{-1}. A large fraction of the initial change takes place within the time resolution of our experiment, < 100 fs, see Table 2, and then decays on different time scales depending on the region in the intermolecular response being considered. There is still a significant difference in the intermolecular response 300 ps after excitation of C102. This difference at comparably long delay times appears to decay on a time scale that is longer than our experiment and consistent with the 4 ns excited-state lifetime of C102 in polar solvents.[72]

While the RaPTORS measurement provides a direct determination of the change in the intermolecular Raman spectrum, $\Delta R^{(3)}(\omega;t)$, reconstruction of the intermolecular spectrum of that fraction of the solvent that experiences a change before and after resonant excitation of C102 from the measured difference,

$$\Delta R^{(3)}(\omega;t) = R^{(3)}_{\text{after}}(\omega;t) - R^{(3)}_{\text{before}}(\omega) \qquad (22)$$

requires knowledge of either $R^{(3)}_{\text{after}}(\omega;t)$ or $R^{(3)}_{\text{before}}(\omega)$ and the absolute magnitude of the change. To illustrate the difference in the response before and after excitation, we can approximate $R^{(3)}_{\text{before}}(\omega)$ as the bulk solvent response, $R^{(3)}_{\text{solvent}}(\omega)$. The magnitude of the change is estimated as 1% at (t = 500 fs, τ = 150 fs) based on the relative intensities of the signal and intrinsic local oscillator, see section 3.3. Combining these estimates with $\Delta R^{(3)}(\omega;t)$ in Figure 6, the resulting $R^{(3)}_{\text{after}}(\omega;t)$ is shown in Figure 8. We note that there is no expectation that the intermolecular spectrum associated with the small fraction of molecules that are affected by the excitation of C102 is identical to the bulk solvent. Those solvent molecules that are affected by the change in C102 must interact with C102 in the ground state and thereby should have a different intermolecular spectrum than solvent far removed from the solute on average. Figure 8 is intended only to illustrate the magnitude of the change as a function of delay time and frequency and indicate how the spectrum shifts in response to C102 excitation.

TABLE 3: Calculated Bimolecular Interaction Energies for C102 in CH_3CN Using Eq 21[a]

	μ/D	α/Å^3	E^I/eV	electrostatic	induction	dispersion
ground state, S_0	9.1	27.2	6.8	−16.7	−0.7	−1.3
excited state, S_1	11.1	29.3	3.7	−24.7	−0.9	−1.4
difference	2.0	2.1	−3.1	−8.0	−0.2	−0.1

[a] Energy values are given in units of 10^{-79} kJ·m^6.

5.1. The Equilibrated Difference in the Intermolecular Response. In Figure 6 the TOR spectrum has, for the most part, stopped evolving by 300 ps after excitation of C102. In this long time limit the change in the response reflects the difference between the equilibrated intermolecular spectrum around the excited and ground states of C102. The change in the intermolecular interaction between C102 and acetonitrile following excitation of C102 is dominated by the increase in the dipole−dipole interaction, see Table 3. The increase in the intermolecular interaction, as reflected by the decrease in the intermolecular potential energy, is expected to increase the local density and tighten the associated solvent−solute and solvent−solvent intermolecular potentials. Although the effects of temperature and density are not strictly independent, temperature-dependent studies of the intermolecular spectrum of neat liquids have demonstrated similar changes as the temperature is reduced with a concomitant increase in the density.[73−77] In these studies, the high-frequency librational motions shift to higher frequencies and collective reorganization shifts to lower frequencies. The increase in frequency and decrease in damping of the librational motions can be attributed to the density increase, due to an increase in the effective force constant associated with librational motion. The increased density will also shift the collision-induced contributions to higher frequencies. The shift of the collective motions to lower frequency with a reduction in temperature can be explained in terms of the increased viscosity[75] or the result of a change in level dependent damping.[73] Our results demonstrate analogous shifts of the intermolecular spectrum following excitation of C102, Figure 8, and we assign these shifts predominantly to an increase in the local density that accompanies the excitation.

In addition to the increase in the dipolar interaction, heating of the local environment may follow excitation due to increased kinetic energy from both the intermolecular solvation events and transfer of excess C102 vibrational energy to the solvent.[16,18,78−81] Temperature-dependent studies of neat CH_3CN indicate that an increase in thermal energy would result in an opposite shift of the intermolecular spectrum than observed in Figure 8.[73] An increase in the temperature would shift the librations to lower frequencies and the diffusive reorganization to higher frequencies. The resulting change in the spectrum would present an increase at intermediate intermolecular frequencies and a decrease at the wings, the opposite of what we observe in Figure 6. Excitation at 400 nm is on the low energy side of the C102 absorption maximum at 380 nm, leaving a limited amount of excess energy for transfer to the solvent. In experiments with the analogous Coumarin dyes C152 and C153, where excitation at 400 nm is near the peak of the absorption for C152 and 1800 cm^{-1} to the high energy side of the maximum in C153, we have observed a dramatic change in

the RaPTORS response. In the case of C153 the response even becomes slightly positive for intermediate intermolecular frequencies.[82] A systematic study of the dependence of the RaPTORS signal on resonant excitation frequency will be required to quantitatively address the shift in the balance between the density increase due to increased intermolecular interactions and the decrease that accompanies increased solvent kinetic energy following energy transfer from the solute. Our results indicate that for excitation of C102 at 400 nm the increase in the electrostatic interaction exerts a larger influence on the local density than any heating due to intra- and intermolecular energy transfer.

5.2. Evolution of the Intermolecular Response. The evolution of the intermolecular spectrum following excitation of C102 can generally be described by a very rapid, <100 fs, initial change followed by a biexponential approach to equilibrium around the excited state of C102. However, each portion of the response is changing on a different time scale. The fits of the raw RaPTORS response along t for different values of τ, Table 2, illustrate how the time dependence varies depending on the portion of the intermolecular response that is probed. All of the τ values in Table 2 are within the portion of the Raman response that has experienced a negative change, as shown in the bottom of Figure 6. At $\tau = 150$ fs, near the peak of the intermolecular response, the two time constants in the evolution, t_2 and t_3 in Table 2 and eq 14, are the smallest. Going to larger or smaller values of τ increases both of the decay times, with t_2 and t_3 becoming progressive longer as τ increases. This trend is the result of the complex shifting of the broad overlapping components in the intermolecular spectrum with time. The initial response shifts the faster portions to earlier times and the slower portions to later times. These responses then start to shift back, finally equilibrating around excited-state C102. Near the peak of the response, the result is an initial loss that fills in with time; however, at points in the spectrum progressively closer to the boundaries of the sign change the combined positive and negative evolutions can lead to a near cancelation, and very little change is exhibited as a function of time. This can be seen near $\tau = 50$ fs and $\tau = 1$ ps in Figure 6.

Decay of the RaPTORS response as a function of t would also be expected to result from rotation of the excited C102 solute due to the anisotropy in the solvent's polarizability and the tensorial nature of the measured response. Solute rotation would produce a decay of the entire RaPTORS response on the same, rotational, time scale with the largest amplitude corresponding to the maximum in the RaPTORS signal at $\tau = 150$ fs. Assuming the rotation time for excited C102 is similar to the measured rotation time for the analogous dye C153 in CH_3CN, 21 ps,[83] neither of the time constants in the decay at $\tau = 150$ fs correspond to rotation. In the fits to the time evolution along t the minimum number of steps required to obtain a reasonable fit were employed, eq 14. Although a 21 ps decay due to rotation could be added to each of the fits along t, the quality of our data was not sufficient to resolve this or any other additional time scales. While solute rotation may contribute to the decay, the different time scales measured at each value of τ, and the lack of consistency with the C102 rotation time, indicate that time-dependent shifting of the intermolecular spectrum plays a significant role in the observed response even at longer delays.

Inspection of Figure 6 demonstrates a complex evolution of the spectrum following excitation of C102. Looking at the higher frequencies, > 100 cm^{-1}, there is a large initial jump within the time resolution of our experiment and then a rapid decay in the first 500 fs after excitation. The time scale is consistent with the initial solvation response previously measured for CH_3CN and is the result of the motions that are driven by the sudden increase in the C102 dipole moment.[9,84,85] However, with the first frequency resolved time point at $t = 250$ fs we are only able to measure the effect of the tail of this portion of the response. Schmuttenmaer and co-worker found a similar transient increase and shift of the high-frequency intermolecular motions in the nondipolar solvation of TBNC.[26,28,86] Using polarizability response spectroscopy, Scherer and co-workers found that translational and collision-induced contributions are preferentially driven by the excitation of C153 in CH_3CN, in agreement with the viscoelastic solvation model of Berg[24,68−70] On the basis of these studies and our observed change in the intermolecular spectrum, we conclude that the sudden increase and rapid sub-picosecond recovery of the higher frequency motions in the RaPTORS response may reflect transient librations, but primarily is the result of translational motion that accompanies an impulsively driven local density fluctuation.

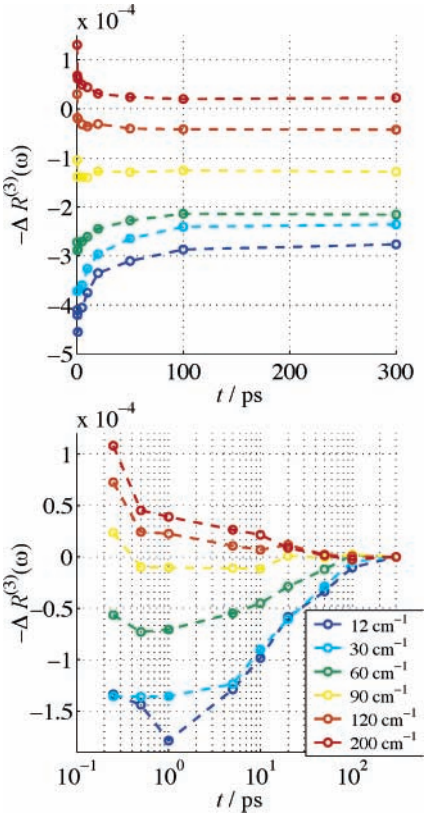

Figure 9. The t dependence for the frequency indicated in the legend from the fits shown in the top of Figure 6 (top). The fits shown in the top plot, with the value at $t = 300$ ps subtracted to highlight the time-dependent evolution (bottom). In both figures the circles are the nine time points along t taken from Figure 6, and the dashed lines simply connect these points.

All of the frequencies in Figure 6 show a large initial, < 250 fs, change, and the subsequent evolution is strongly dependent on the frequency. While the higher frequencies demonstrate a rapid decay, intermediate frequencies show much smaller changes during the first picosecond with the spectral evolution in this region appearing to get a later start. Figure 9 illustrates how various points in the intermolecular spectrum are changing in time. In the bottom of Figure 9 the dynamic evolution of different frequencies is highlighted by subtracting the value at 300 ps for each frequency, where we assume the solvent has effectively reached equilibrium around the excited state of C102. Frequencies greater than 60 cm^{-1} have a rapid decline between

$t = 250$ fs and $t = 500$ fs, with over half of the dynamic response for frequencies above 100 cm^{-1} completed within the first picosecond. In contrast, there is very little evolution at 30 cm^{-1} during the first 5 ps, and the majority of the change takes place between 5 and 100 ps.

The last period of evolution in the intermolecular spectrum takes place on a 48 ps to 100 ps time scale, see Table 2, and it accounts for a large fraction of the spectral evolution for frequencies below 40 cm^{-1}. This is much slower than the solvation time scales observed using a resonant probe of the solute, where the solvation was characterized by a biexponential response involving 89 and 630 fs decays.[9,57,85] Given that in Figure 9 a significant portion of the fastest, < 200 fs, response has been missed with the earliest resolvable point at a delay of $t = 250$ fs, the responses of the highest frequencies are similar to the resonant measurements with a significant sub-picosecond contribution. The sub-picosecond components that dominates the response in the resonant measurements reflect the strong influence of the closest solvent molecules, the first solvation shell, on the electronic energy of the solute.[18] Now consider the dramatic dependence of the observed response on the frequency. At 30 cm^{-1} the entire evolution takes place on a significantly longer time scale than observed in the resonant measurements. The nonresonant solvent probe lacks any inherent bias based on proximity to the solute. This suggests that the slower changes that are dominant at lower frequencies reflect reorganization over larger distances than are probed in resonant solute measurements. As a result, a qualitative connection between the frequency and the length scale of the motion being probed can be drawn. However, Figure 9 also shows that even at higher frequencies there is a slow decay component, albeit a much smaller relative contribution than at lower frequencies. This is evidence of the complex relationship between the length scale and the frequency and a more quantitative interpretation of our results in terms of changes in the wavevector and frequency dependent response will require molecular simulations.[87] One possible explanation for the slow response that appears over longer length scales would be the transfer of excess potential energy to thermal (kinetic) energy of the surrounding solvent. Maroncelli has considered this in detail with MD simulations, demonstrating that following a very rapid jump in the kinetic energy of the first solvation shell, the energy is transferred to ever greater distances from the solute on ever slower time scales.[16] As discussed in Section 5.1, an increase in the effective thermal temperature of the solvent would increase the response at frequencies below 60 cm^{-1}.

5.3. Comparison with Linear Response. The application of linear response to solvation requires that the perturbation to the solvent from excitation of the solute is small, and thus the response of the solvent is equivalent to the statistical fluctuations in the absence of the perturbation.[14] When applied to the nonequilibrium dynamics of the solute electronic energy gap, $S(t)$, this means that LR requires that the equilibrium solvent fluctuations in the presence of the excited state of the chromophore are the same as the fluctuations in the presence of the ground state. Computational studies have shown that this is not the case for significant changes in solute charge distribution, and the results presented here provide direct experimental confirmation that this is not the case for excitation of C102 in acetonitrile.[10,11,14−17] Figures 6 and 8 clearly demonstrate that there is a significant change in the equilibrated spectrum of intermolecular motions following excitation. On the basis of this experimental observation, failure of LR is expected when attempting to use the statistical fluctuations about the ground-state solute, $C_{gs}(t)$, to predict $S(t)$.

Simulations have found that LR applied to predictions of $S(t)$ does a good job for the fastest components of the solvent response, <100 fs. This has been explained by the fact that the response is dominated by inertial motions, i.e., it is dictated by motion prior to the perturbation.[10,14] Our current time resolution is not sufficient to address these earliest events in detail. However, the slower response in $S(t)$ observed in the simulations, ca. 1 ps, was found to be poorly predicted by $C_{gs}(t)$.[14,16] Our results indicate that following a large <100 fs change in the spectrum, there is limited evolution of the most intense center of the intermolecular spectrum during the first picosecond. Following the inertial motions, the solvent fluctuations during this period reflect the new, pseudo-equilibrated intermolecular response about the excited chromophore. The difference in the solvent spectrum between the ground and excited state solute at this point is actually larger than it is after subsequent equilibration takes place. The longest time scale of intermolecular spectral evolution that we observe, 50 ps to 100 ps, is most apparent for frequencies below 60 cm^{-1} and actually shows a modest reduction of the difference. These time scales are not observed in the resonant solvation experiments, and simulations have not yet addressed these extended time scales. If, as we have proposed, this evolution represents changes over larger distances from the chromophore as the result of thermal energy transfer, then the effect on the solute's electronic energy should be small. Under these conditions deviations from LR would be indicated by the difference in the local solvent fluctuations established prior to the longer time scales associated with the thermal energy transfer chain and therefore would suggest even slightly larger deviations from LR than would be predicted from the differences in the fully equilibrated solvent response about the ground and excited states.

6. Conclusion

We have demonstrated the application of a new technique to directly measure the change in the entire intermolecular Raman spectrum and its dynamic evolution, following excitation of a chromophore in solution. This technique was applied to examine the dipolar solvation event that follows excitation of C102 in acetonitrile. After excitation of C102, the spectrum demonstrated a complex bifurcation, where the higher frequency components broaden and shift higher in frequency, and the lower frequency components shift to lower frequencies. This is attributed to the increased local solvent density that accompanies the increased dipolar solvent−solute interaction. Following an initial, <100 fs, change, evolution of the spectrum is strongly frequency dependent, with a large fraction of the equilibration around the excited state at high frequencies taking place in less than a picosecond. In contrast, lower frequency components equilibrate more slowly, with very little relaxation during the first picosecond after excitation. Comparison with resonant solvation experiments by others suggests a connection between the frequency and length scale of the response, with changes at lower frequencies probing the change in the response at larger distances from the chromophore. The slowest changes at lower frequencies is likely the result of intermolecular kinetic (thermal) energy transfer to subsequently greater distances from the solute and is not seen in the resonant solvation measurements.

Unlike resonant probes of solvation dynamics, which probe the nonequilibrium evolution of the electronic energy gap, the RaPTOR S experiment is a direct probe of the *change* in the local solvent response relative to the ground electronic state of

the chromophore. To our knowledge, these measurements provide the first direct measurements of the difference between the solvent fluctuations around the ground and excited electronic states of the chromophore for a dipolar solvation event. For the large change in the C102 dipole moment, the difference is significant. The large change in equilibrium solvent fluctuations agrees with molecular dynamics simulations[14,16] and, along with the time-dependent evolution of the solvent response, provides experimental confirmation of a failure of linear response in dipolar solvation. The results also indicate that after the inertial response the solvent fluctuations are well represented by the equilibrium dynamics around the excited state of the chromophore, as one might expect.

The experiments here have demonstrated that the spectrum of fluctuations in the local solvent environment undergo significant changes as charge is redistributed in a solute. The changing local intermolecular response has important implications for understanding solvation and the dynamics associated with reactive events in solution as the local intermolecular environment evolves through the transition from reactant to product. This includes the complicated dynamics associated with intermolecular thermal energy transfer. We have demonstrated a new technique capable of following these changes, and one of the strengths of this technique is the separation of the solvent probe from spectroscopy of the solute. Future applications should provide details of how dynamic changes in the local environment participate in condensed phase reactive events.

Acknowledgment. This work was supported by NSF under Award Number CHE-0211894 and was supported in part by the MRSEC Program of the NSF under Award Number DMR-0212302. D.B. gratefully acknowledges support from the Camille and Henry Dreyfus Foundation, the David and Lucille Packard Foundation, and the 3M company for their generous support. D.F.U. thanks the Minnesota Supercomputing Institute for computing time, resources, and travel funding.

Note Added after ASAP Publication. This article was published on Articles ASAP on March 24, 2005, with an error in the denominator of eq 6. The corrected version was posted March 28, 2005.

Supporting Information Available: Fitting parameters, all data, and all fits. This material is available free of charge via the Internet at http://pubs.acs.org.

References and Notes

(1) Rossky, P. J.; Simon, J. D. *Nature (London)* **1994**, *370* (6487), 263−9.

(2) Heitele, H. *Angew. Chem.* **1993**, *105* (3), 378−98 (See also *Angew. Chem., Int. Ed. Engl.* **1993**, *32* (3), 359−77).

(3) Barbara, P. F.; Meyer, T. J.; Ratner, M. A. *J. Phys. Chem.* **1996**, *100* (31), 13148−13168.

(4) Reichardt, C. *Solvents and Solvent Effects in Organic Chemistry*, 3rd ed.; Wiley−VCH: New York, 2003.

(5) Barbara, P. F.; Jarzeba, W. *Adv. Photochem.* **1990**, *15*, 1−68.

(6) De Boeij, W. P.; Pshenichnikov, M. S.; Wiersma, D. A. *Annu. Rev. Phys. Chem.* **1998**, *49*, 99−123.

(7) Fleming, G. R.; Cho, M. *Annu. Rev. Phys. Chem.* **1996**, *47*, 109−134.

(8) Gardecki, J.; Horng, M. L.; Papazyan, A.; Maroncelli, M. *J. Mol. Liq.* **1995**, *65/66*, 49−57.

(9) Horng, M. L.; Gardecki, J. A.; Papazyan, A.; Maroncelli, M. *J. Phys. Chem.* **1995**, *99*, 17311−17337.

(10) Carter, E. A.; Hynes, J. T. *J. Chem. Phys.* **1991**, *94* (9), 5961−5979.

(11) Bedard-Hearn, M. J.; Larsen, R. E.; Schwartz, B. J. *J. Phys. Chem. A* **2003**, *107* (24), 4773−4777.

(12) Cammi, R.; Mennucci, B. *J. Chem. Phys.* **1999**, *110* (20), 9877−9886.

(13) Aaqvist, J.; Hansson, T. *J. Phys. Chem.* **1996**, *100*, 0 (22), 9512−9521.

(14) Fonseca, T.; Ladanyi, B. M. *J. Phys. Chem.* **1991**, *95*, 5(6), 2116−19.

(15) Fonseca, T.; Ladanyi, B. M. *J. Mol. Liq.* **1994**, *60*, 1−24.

(16) Maroncelli, M. *J. Chem. Phys.* **1991**, *94* (3), 2084−103.

(17) Aherne, D.; Tran, V.; Schwartz, B. J. *J. Phys. Chem. B* **2000**, *104* (22), 5382−5394.

(18) Ladanyi, B. M.; Maroncelli, M. *J. Chem. Phys.* **1998**, *109* (8), 3204−3221.

(19) Day, T. J. F.; Patey, G. N. *J. Chem. Phys.* **1999**, *110* (22), 10937−10944.

(20) Ladanyi, B. M.; Perng, B.-C. *J. Phys. Chem. A* **2002**, *106* (30), 6922−6934.

(21) Beard, M. C.; Turner, G. M.; Schmuttenmaer, C. A. *J. Phys. Chem. B* **2002**, *106* (29), 7146−7159.

(22) Haran, G.; Sun, W. D.; Wynne, K.; Hochstrasser, R. M. *Chem. Phys. Lett.* **1997**, *274* (4), 365−371.

(23) Haran, G.; Sun, W. D.; Wynne, K.; Hochstrasser, R. M. *Chem. Phys. Lett.* **1997**, *277* (5−6), 579.

(24) Park, S.; Flanders, B. N.; Shang, X.; Westervelt, R. A.; Kim, J.; Scherer, N. F. *J. Chem. Phys.* **2003**, *118* (9), 3917−3920.

(25) Beard, M. C.; Turner, G. M.; Schmuttenmaer, C. A. *J. Phys. Chem. A* **2002**, *106* (6), 878−883.

(26) Beard, M. C.; Turner, G. M.; Schmuttenmaer, C. A. *ACS Symp. Ser.* **2002**, *820* (Liquid Dynamics), 44−57.

(27) Schmuttenmaer, C. A. *Sci. Prog. (Northwood, U.K.)* **2002**, *85* (2), 175−197.

(28) Schmuttenmaer, C. A. *Chem. Rev. (Washington, D. C.)* **2004**, *104* (4), 1759−1779.

(29) Underwood, D. F.; Blank, D. A. *J. Phys. Chem. A* **2003**, *107* (7), 956−961; see also: *J. Phys. Chem. A* **2003**, *107* (45), 9736.

(30) Schmidtke, S. J.; Underwood, D. F.; Blank, D. A. *J. Am. Chem. Soc.* **2004**, *126* (28), 8620−8621.

(31) Underwood, D. F.; Blank, D. A. *Trends Opt. Photonics (Thirteenth International Conference on Ultrafast Phenomena)* **2002**, *72*.

(32) Underwood, D. F.; Blank, D. A. *Trends Opt. Photonics (Fourteenth International Conference on Ultrafast Phenomena)* **2004**, in press.

(33) Etchepare, J.; Grillon, G.; Chambaret, J. P.; Hamoniaux, G.; Orszag, A. *Opt. Commun.* **1987**, *63* (5), 329−34.

(34) Hellwarth, R. W. *Prog. Quantum Electron.* **1977**, *5* (Pt. 1), 1−68.

(35) Khalil, M.; Demirdöven, N.; Golonzka, O.; Fecko, C. J.; Tokmakoff, A. *J. Phys. Chem. A* **2000**, *104* (24), 5711−5715.

(36) Goodno, G. D.; Dadusc, G.; Miller, R. J. D. *J. Opt. Soc. Am. B* **1998**, *15* (6), 1791−1794.

(37) Maznev, A. A.; Nelson, K. A.; Rogers, A. *Opt. Lett.* **1998**, *23* (16), 1319−1321.

(38) Gaussian 98 (Revision a.11). Frisch, M. J.; Trucks, G. W.; Schlegel, B. H.; Scuseria, G. E.; Robb, M. A.; Cheeseman, J. R.; Zakrzewski, V. G.; J. A. Montgomery, J.; Stratmann, R. E.; Burant, J. C.; Dapprich, S.; Millam, J. M.; Daniels, A. D.; Kudin, K. N.; Strain, M. C.; Farkas, O.; Tomasi, J.; Barone, V.; Cossi, M.; Cammi, R.; Mennucci, B.; Pomelli, C.; Adamo, C.; Clifford, S.; Ochterski, J.; Petersson, G. A.; Ayala, P. Y.; Cui, Q.; Morokuma, K.; Salvador, P.; Dannenberg, J. J.; Malick, D. K.; Rabuck, A. D.; Raghavachari, K.; Foresman, J. B.; Cioslowski, J.; Ortiz, J. V.; Baboul, A. G.; Stefanov, B. B.; Liu, G.; Liashenko, A.; Piskorz, P.; Komaromi, I.; Gomperts, R.; Martin, R. L.; Fox, D. J.; Keith, T.; Al-Laham, M. A.; Peng, C. Y.; Nanayakkara, A.; Challacombe, M.; Gill, P. M. W.; Johnson, B.; Chen, W.; Wong, M. W.; Andres, J. L.; Gonzalez, C.; Head-Gordon, M.; Replogle, E. S.; J. A. Pople, Gaussian, Inc., Pittsburgh, PA, 2001.

(39) ZINDO-MN, version 1.1. Zerner, M.; Ridley, J.; Bacon, A.; Head, J.; Edwards, W.; Head, J.; McKelvey, J.; Cuberson, J.; Knappe, P.; Cory, M.; Weiner, B.; Baker, J.; Parkinson, W.; Kannis, D.; Yu, J.; Roesch, N.; Kotzian, M.; Tamm, T.; Karelson, M.; Zheng, X.; Pearl, G.; Broo, A.; Albert, K.; Cullen, J.; Li, J.; Hawkins, G.; Thompson, J.; Liotard, D.; Cramer, C.; Truhlar, D. G., Quantum Theory and Project, University of Florida, Gainesville, and Department of Chemistry, University of Minnesota, Minneapolis, 2002.

(40) Mukamel, S. *Principles of nonlinear optical spectroscopy*; Oxford University Press: New York, 1995.

(41) Yan, Y.-x.; Nelson, K. A. *J. Chem. Phys.* **1987**, *87* (11), 6240−6256.

(42) Smith, N. A.; Meech, S. R. *Int. Rev. Phys. Chem.* **2002**, *21* (1), 75−100.

(43) Ruhman, S.; Joly, A. G.; Nelson, K. A. *IEEE J. Quantum Electron.* **1988**, *24* (2), 460−469.

(44) McMorrow, D.; Lotshaw, W. T. *J. Phys. Chem.* **1991**, *95*, 5(25), 10395−406.

(45) McMorrow, D.; Lotshaw, W. T.; Kenney-Wallace, G. A. *IEEE J. Quantum Electron.* **1988**, *QE-24* (2), 443−54.

(46) Cho, M.; Du, M.; Scherer, N. F.; Fleming, G. R.; Mukamel, S. *J. Chem. Phys.* **1993**, *99* (4), 2410−2428.

(47) Ruhman, S.; Joly, A. G.; Nelson, K. A. *J. Chem. Phys.* **1987**, *86* (11), 6563−6565.
(48) McMorrow, D.; Thantu, N.; Melinger, J. S.; Kim, S. K.; Lotshaw, W. T. *J. Phys. Chem.* **1996**, *100* (24), 10389−10399.
(49) Lotshaw, W. T.; McMorrow, D.; Thantu, N.; Melinger, J. S.; Kitchenham, R. *J. Raman Specrosc.* **1995**, *26*, 571−583.
(50) Murry, R. L.; Fourkas, J. T. *J. Chem. Phys.* **1997**, *107* (23), 9726−9740.
(51) Vohringer, P.; Scherer, N. F. *J. Phys. Chem.* **1995**, *99* (9), 2684−2695.
(52) Maitland, G. C.; Rigby, M.; Smith, E. B.; Wakeham, W. A. *Intermolecular Forces. Their Origin and Determination*; Clarendon Press: Oxford, 1987.
(53) Huyskens, P. L.; Luck, W. A. P.; Zeegers-Huyskens, T. *Intermolecular Forces: An Introduction to Modern Methods and Results*; Springer-Verlag: New York, 1991.
(54) Cave, R. J.; Castner, Edward W., J. *J. Phys. Chem. A* **2002**, *106* (50), 12117−12123.
(55) Caricato, M.; Mennucci, B.; Tomasi, J. *J. Phys. Chem. A* **2004**, *108* (29), 6248−6256.
(56) McCarthy, P. K.; Blanchard, G. J. *J. Phys. Chem.* **1993**, *97*, 7(47), 12205−9.
(57) Rosenthal, S. J.; Jimenez, R.; Fleming, G. R.; Kumar, P. V.; Maroncelli, M. *J. Mol. Liq.* **1994**, *60*, 25−56.
(58) Kumar, P. V.; Maroncelli, M. *J. Chem. Phys.* **1995**, *103* (8), 3038−3060.
(59) Maroncelli, M.; Kumar, V. P.; Papazyan, A. *J. Phys. Chem.* **1993**, *97*, 7(1), 13−17.
(60) Ladanyi, B. M.; Klein, S. *J. Chem. Phys.* **1996**, *105* (4), 1552−1561.
(61) Ladanyi, B. M.; Liang, Y. Q. *J. Chem. Phys.* **1995**, *103* (15), 6325−6332.
(62) Frenkel, D.; McTague, J. P. *J. Chem. Phys.* **1979**, *72* (4), 2801−2818.
(63) Steele, W. *Mol. Phys.* **1987**, *61*, 1031.
(64) Saito, S.; Ohmine, I. *J. Chem. Phys.* **1997**, *106* (12), 4889−4893.
(65) Murry, R. L.; Fourkas, J. T.; Keyes, T. *J. Chem. Phys.* **1998**, *109* (7), 2814−2825.
(66) Madden, P. A.; Cox, T. I. *Mol. Phys.* **1981**, *43* (2), 287−305.
(67) Kivelson, D.; Madden, P. A. *Annu. Rev. Phys. Chem.* **1980**, *31*, 523−558.
(68) Berg, M. *J. Phys. Chem. A* **1998**, *102* (1), 17−30.
(69) Berg, M. A.; Hubble, H. W. *Chem. Phys.* **1998**, *233* (2, 3), 257−266.
(70) Berg, M. A. *J. Chem. Phys.* **1999**, *110* (17), 8577−8588.
(71) Larsen, D. S.; Ohta, K.; Fleming, G. R. *J. Chem. Phys.* **1999**, *111* (19), 8970−8979.
(72) Hou, Y.; Ming, C.; Zhou, D.; Wang, W. *Yingyong Huaxue* **1987**, *4* (4), 53−7.
(73) Farrer, R. A.; Loughnane, B. J.; Deschenes, L. A.; Fourkas, J. T. *J. Chem. Phys.* **1997**, *106* (17), 6901−6915.
(74) Ruhman, S.; Kohler, B.; Joly, A. G.; Nelson, K. A. *Chem. Phys. Lett.* **1987**, *141* (1, 2), 16−24.
(75) Tokmakoff, A.; Lang, M. J.; Jordanides, X. J.; Fleming, G. R. *Chem. Phys.* **1998**, *233* (2−3), 231−242.
(76) Ji, X.; Ahlborn, H.; Space, B.; Moore, P. B. *J. Chem. Phys.* **2000**, *113* (19), 8693−8699.
(77) Moore, P.; Keyes, T. *J. Chem. Phys.* **1994**, *100* (9), 6709−17.
(78) Wang, Z.; Pakoulev, A.; Dlott, D. D. *Science (Washington, D. C.)* **2002**, *296* (5576), 2201−2203.
(79) Stratt, R. M.; Maroncelli, M. *J. Phys. Chem.* **1996**, *100* (31), 12981−12996.
(80) Owrutsky, J. C.; Raftery, D.; Hochstrasser, R. M. *Annu. Rev. Phys. Chem.* **1994**, *45*, 519−55.
(81) Elsaesser, T.; Kaiser, W. *Annu. Rev. Phys. Chem.* **1991**, *42*, 83−107.
(82) Underwood, D. F.; Blank, D. A. Unpublished results.
(83) Horng, M. L.; Gardecki, J. A.; Maroncelli, M. *J. Phys. Chem. A* **1997**, *101* (6), 1030−1047.
(84) Cho, M.; Rosenthal, S. J.; Scherer, N. F.; Ziegler, L. D.; Fleming, G. R. *J. Chem. Phys.* **1992**, *96* (7), 5033−8.
(85) Rosenthal, S. J.; Xie, X.; Du, M.; Fleming, G. R. *J. Chem. Phys.* **1991**, *95* (6), 4715−18.
(86) Venables, D. S.; Schmuttenmaer, C. A. *Springer Ser. Chem. Phys.* **1998**, *63* (Ultrafast Phenomena XI), 565−567.
(87) Bagchi, B.; Biswas, R. *Adv. Chem. Phys.* **1999**, *109*, 207−433.